Quasi-two-dimensional spin distributions in II-VI magnetic semiconductor heterostructures: Clustering and dimensionality

S. A. Crooker
National High Magnetic Field Laboratory, MS E536, Los Alamos, New Mexico 87545

N. Samarth
Department of Physics, Pennsylvania State University, University Park, Pennsylvania 16802

D. D. Awschalom
Department of Physics, University of California, Santa Barbara, California 93106
(Received 19 July 1999)

Spin clustering in diluted magnetic semiconductors (DMS) arises from antiferromagnetic exchange between neighboring magnetic cations and is a strong function of reduced dimensionality. Epitaxially grown single monolayers and abrupt interfaces of DMS are, however, never perfectly two dimensional (2D) due to the unavoidable intermonolayer mixing of atoms during growth. Thus the magnetization of DMS heterostructures, which is strongly modified by spin clustering, is intermediate between that of 2D and 3D spin distributions. We present an exact calculation of spin clustering applicable to *arbitrary* distributions of magnetic spins in the growth direction. The results reveal a surprising insensitivity of the magnetization to the form of the intermixing profile, and identify important limits on the maximum possible magnetization. High-field optical studies of heterostructures containing ''quasi-2D'' spin distributions are compared with calculation.

Spin clustering is ubiquitous in II-VI diluted magnetic semiconductors (DMS), resulting in reduced effective magnetizations at low magnetic fields and magnetization steps at high fields.[1] Clear predictions can be made for the number and type of spin clusters in 3D systems (e.g., bulk $Cd_{1-x}Mn_xSe$), where the distribution of magnetic Mn^{2+} cations is random and isotropic. With the advent of molecular-beam epitaxy (MBE) and other techniques for monolayer-by-monolayer growth of DMS heterostructures, spin clustering in systems of reduced dimensionality has enjoyed much recent interest. It is well established[2–5] that spin clustering (arising mainly from an antiferromagnetic exchange between neighboring magnetic cations) should be greatly reduced in two-dimensional systems such as abrupt interfaces or discrete monolayer planes, leading to enhanced paramagnetism. However, experiments show[2–5] that perfect 2D interfaces and monolayers are never realized due to the inevitable intermonolayer mixing of atoms during MBE growth, which smears the magnetic cations over several monolayers. Common mechanisms include segregation (mixing between the monolayer being grown and the underlying monolayer) which leads to roughly exponential magnetic profiles, and diffusion (which can arise from, e.g., high growth temperatures or annealing) which leads to gaussian profiles. Hence, real DMS heterostructures are more accurately said to contain ''quasi-2D'' distributions of spins, with a corresponding magnetization and degree of spin clustering somewhere between that of bulk (3D) and planar (2D) spin distributions.

The local, planar magnetic concentration in these quasi-2D spin distributions varies significantly from monolayer to monolayer, strongly affecting the probability of forming spin clusters (which themselves may span many monolayers). It is desirable to quantitatively predict the degree of this spin clustering in a given DMS heterostructure so that accurate comparisons can be made with real data. In this paper, we present exact expressions for determining the number and type of spin clusters (singles, pairs, open and closed triples) for *arbitrary* distributions of magnetic spins in the common (100) growth direction. The results reveal a rather surprising insensitivity of the computed magnetization to the form of the intermixing profile (exponential/gaussian), and highlight important limits on the maximum possible magnetization using MBE techniques. High-field photoluminescence (PL) and reflectivity studies of DMS superlattices and quantum wells containing quasi-2D magnetic planes are compared with the analytic results.

Spin clustering in DMS derives predominantly from the strong antiferromagnetic *d-d* exchange between nearest-neighbor (NN) magnetic cations ($J_{NN} \sim -10$ K). As outlined in the work of Shapira[1] and others,[6] single Mn^{2+} cations with no magnetic NN's are $S=\frac{5}{2}$ paramagnets, with Brillouin-like magnetization. Two NN Mn^{2+} cations form an antiferromagnetically locked pair with zero spin at low magnetic fields, and steplike magnetization at high fields and low temperatures. Three Mn^{2+} spins can form a closed or open triple with net spin $S_T=\frac{1}{2}$ and $S_T=\frac{5}{2}$ (respectively) at low fields, and a unique set of magnetization steps at high fields.[6] Spins in higher order clusters are usually treated empirically and often exhibit a linear susceptibility at high magnetic fields.[1]

The magnetization of monolayer planes of Mn^{2+} spins is a significant challenge for conventional magnetometery. Alternatively, the magnetization from DMS heterostructures may be inferred from their giant magneto-optical properties. The $J_{sp\text{-}d}$ exchange interaction between electrons/holes and local Mn^{2+} moments generates giant exciton spin splittings that are proportional to the *local* magnetization within the exciton wave function. Using the giant spin splitting of confined excitons to probe the magnetization within a quantum

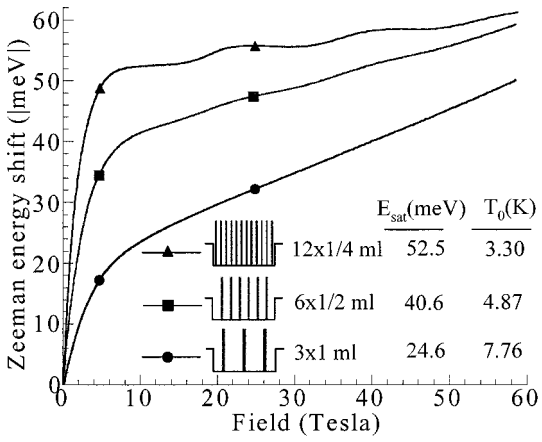

FIG. 1. Measured energy shift (abs. value) of the exciton PL to 60 T at 350 mK in three quantum wells containing the *same number* of Mn^{2+} spins, but in different quasi-2D distributions, showing increased spin clustering with increasing 2D concentration.

well, the studies of Gaj,[3] Grieshaber,[2] and of Ossau[4] clearly established (i) an enhanced paramagnetic response in very thin layers of magnetic semiconductor, and (ii) that ''ideal'' magnetic-nonmagnetic semiconductor interfaces are smeared out due to segregation of Mn^{2+} during growth. A clear example of both effects can be seen in the high-field PL data of Fig. 1. Here, we measure the giant energy shift ($\propto$ magnetization) of the band-edge exciton PL to 60 Tesla in three quantum wells, each containing the *same total number* of Mn^{2+} spins, but in very different *distributions*. The samples are 120 Å $ZnSe/Zn_{.8}Cd_{.2}Se$ single quantum wells into which the magnetic semiconductor MnSe has been incorporated in the form of ''digital'' planes of 25%, 50%, and 100% monolayer coverage (12, 6, and 3 planes, respectively). The samples and the experimental method have been described elsewhere.[7] Evidence of decreased spin clustering with decreasing planar concentration is clear in the low-field magnetization ($H<8$ T), which is largely due to isolated Mn^{2+} spins and is fit to a modified Brillouin function, $\Delta E = E_{\rm sat} B_{5/2}[5\mu_B H/k_B(T+T_0)]$. $E_{\rm sat}$ is the saturation splitting and T_0 is an empirical parameter that accounts for long-range Mn-Mn interactions.[8] As shown, as the planar Mn^{2+} density increases, $E_{\rm sat}$ decreases while T_0 grows, consistent with the expectation that increasing the planar density results in fewer single (unclustered) Mn^{2+} spins and more long-range correlations between Mn^{2+} spins. Further, with increasing planar density, the high-field susceptibility evolves from magnetization steps (from Mn-Mn pairs), to the linear susceptibility common in large, highly correlated spin clusters. The presence of low-field paramagnetism in the 100% MnSe planes suggest, however, the quasi-2D nature of these spin distributions: a full (perfect) 2D magnetic monolayer would behave as one infinite cluster and contain no paramagnetic spins whatsoever.

The probability of forming a particular spin cluster is essentially determined by the number of (possibly magnetic) NN's bordering the cluster, and the number of ways the cluster can form. In the zinc-blende crystal structure we consider, cations form an fcc lattice, with twelve NN's per cation. Thus the probability of a Mn^{2+} being single or paired in bulk crystals (3D) is $P_s^{3D}=(1-x)^{12}$ and $P_p^{3D}=12x(1-x)^{18}$, respectively, where x is the Mn^{2+} concentration. For perfect 2D monolayers grown in the (100) direction, the cations form a 2D square lattice with only four possible magnetic NN's per cation, so that $P_s^{2D}=(1-x)^4$ and $P_p^{2D}=4x(1-x)^6$. In a real system, the effects of diffusion and/or segregation intermix adjacent monolayers, so that a ''perfect'' 2D plane of DMS is smeared over several monolayers, with the nth (100) monolayer having a 2D magnetic concentration x_n (assumed to be random within the plane). Clustering within these quasi-2D spin distributions can be modeled numerically[9,4] or through analytic approximations,[2] but an exact expression has been lacking. Figure 2 shows the exact probabilities of a Mn^{2+} spin in the nth monolayer belonging to a single, pair, closed, and open triple. Diagrams show the clusters under consideration—e.g., there are three different types of Mn^{2+} pairs (with the paired spin in the $n-1$th, nth or $n+1$th monolayer), each four-fold degenerate. There are four types of closed triples (for a total of 24), and 126 total configurations for open triples. (We do not attempt the 1900 configurations of spin quartets that have been recently identified in the bulk,[10] nor do we consider the much weaker distant-neighbor couplings between Mn^{2+} moments.[11])

This algorithm allows for an exact calculation of spin clusters in a heterostructure with an *arbitrary* distribution of

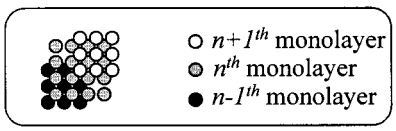

Singles: $y_n^4 y_{n+1}^4 y_{n-1}^4$ (where $y_n = 1-x_n$)

Pairs: $4x_n y_n^6 y_{n+1}^6 y_{n-1}^6 + 4x_{n+1} y_n^5 y_{n-1}^4 y_{n+1}^5 y_{n+2}^4 + 4x_{n-1} y_n^5 y_{n+1}^4 y_{n-1}^5 y_{n-2}^4$

Closed triples: $4x_{n+1}^2 y_{n-1}^4 y_n^6 y_{n+1}^6 y_{n+2}^6 + 4x_{n-1}^2 y_{n+1}^4 y_n^6 y_{n-1}^6 y_{n-2}^6 + 8x_n x_{n+1} y_{n-1}^6 y_n^6 y_{n+1}^6 y_{n+2}^4 + 8x_n x_{n-1} y_{n+1}^6 y_n^6 y_{n-1}^6 y_{n-2}^4$

Open triples: $6x_n^2 y_n^8 y_{n+1}^8 y_{n-1}^8 + 12x_n^2 y_n^7 y_{n+1}^8 y_{n-1}^8 + 16x_n x_{n-1} y_n^7 y_{n+1}^6 y_{n-1}^7 y_{n-2}^4 + 16x_n x_{n+1} y_n^7 y_{n-1}^6 y_{n+1}^7 y_{n+2}^4 + \ldots$

$8x_{n-1}^2 y_n^7 y_{n+1}^4 y_{n-1}^7 y_{n-2}^6 + 8x_{n+1}^2 y_n^7 y_{n-1}^4 y_{n+1}^7 y_{n+2}^6 + 2x_{n-1}^2 y_n^6 y_{n+1}^4 y_{n-1}^6 y_{n-2}^7 + 2x_{n+1}^2 y_n^6 y_{n-1}^4 y_{n+1}^6 y_{n+2}^7 + 4x_{n-1} x_{n+1} y_n^6 y_{n-1}^5 y_{n+1}^5 y_{n-2}^4 y_{n+2}^4 +$
$4x_n x_{n-1} y_n^6 y_{n+1}^7 y_{n-1}^6 y_{n-2}^4 + 4x_n x_{n+1} y_n^6 y_{n-1}^7 y_{n+1}^6 y_{n+2}^4 + 12x_{n+1} x_{n+2} y_{n-1}^4 y_n^5 y_{n+1}^6 y_{n+2}^5 y_{n+3}^4 + 12x_{n-1} x_{n-2} y_{n+1}^4 y_n^5 y_{n-1}^6 y_{n-2}^5 y_{n-3}^4 +$
$8x_{n+1} x_{n-1} y_n^6 y_{n-1}^5 y_{n+1}^5 y_{n-2}^4 y_{n+2}^4 + 4x_{n-1} x_{n-2} y_{n+1}^4 y_n^5 y_{n-1}^5 y_{n-2}^5 y_{n-3}^4 + 4x_{n+1} x_{n+2} y_{n-1}^4 y_n^5 y_{n+1}^5 y_{n+2}^5 y_{n+3}^4 + 4x_{n+1} x_{n-1} y_n^5 y_{n-1}^5 y_{n+1}^5 y_{n-2}^4 y_{n+2}^4$

FIG. 2. Probability of clustering for a spin in the nth (100) monolayer of an arbitrary Mn^{2+} distribution. Multiplying by x_n gives the *number* of clustered spins. Cations in the $n+1$th, nth, and $n-1$th monolayer are labeled by white, shaded, and black dots, respectively.

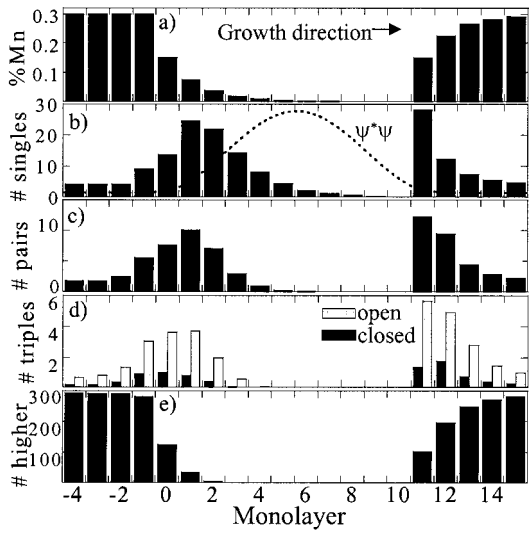

FIG. 3. (a) Schematic of the Mn^{2+} concentration, including segregation effects, in a 10 monolayer-wide quantum well with $x_{Mn}=30\%$ magnetic barriers. (b)–(e) The calculated number of Mn^{2+} cations (per thousand sites) in singles, pairs, open/closed triples, and higher order spin clusters.

Mn^{2+} in the (100) direction. An example of its utility is shown in Fig. 3, where we compute the number of Mn^{2+} in singles, pairs, triples, and higher-order clusters in a 10 monolayer (10 ml) wide nonmagnetic quantum well with magnetic ($x_{Mn}=30\%$) barriers. We assume full segregation of atoms during growth, giving $e^{-n/\lambda}$ and $1-e^{-n/\lambda}$ Mn^{2+} profiles ($\lambda \sim 1.44$ ml) at the first and second interfaces [Fig. 3(a)]. Figures 3(b)–3(e) show the type and number of clusters in each monolayer. Although the Mn^{2+} density is comparatively small near the center of the quantum well, the paramagnetic contribution from single spins to the *optically measured* magnetization can be significant, as it depends on their overlap with the exciton wavefunction as shown. The density of triples and of pairs is clearly peaked in the quasi-2D interfaces. In the barriers, the spin distribution is bulklike and the vast majority of spins are bound up in higher order clusters that contribute little to the low-field magnetization.

Modeling quasi-2D spin distributions leads to some rather unexpected results. In particular, it is clear that magnetization studies alone will be of limited use in distinguishing the exact *form* of the intermixing profile. Figure 4(a) shows the calculated magnetization for four different profiles of an initially 2D monolayer containing 20% Mn^{2+}, where we include the magnetization from singles, pairs, triples, and higher-order clusters following Refs. 1 and 6. Though unrealistic, the first two profiles—a perfect 2D plane with $x_{Mn}=20\%$ and two adjacent planes with $x_{Mn}=10\%$—illustrate an important point: clustering often ''conspires'' to equalize low-field magnetizations. Although the single monolayer contains 5% fewer single Mn^{2+} spins, it contains over a third *more* open triples and higher-order clusters, which act to equalize the deficit. Only at the first magnetization step are the profiles distinguishable, as the single monolayer contains fewer Mn-Mn pairs. The last two profiles represent the exponential and gaussian profiles roughly expected from segregation and diffusion, respectively, with decay length and half-width equal to 1 ml. Again, the calculated magnetizations are nearly identical (although larger than for the first two profiles). Thus, magnetization measurements alone cannot distinguish the form of the spin profile. However, *assuming* a particular form, the magnetization does depend sensitively on the segregation (or diffusion) length, which can then be used to fit an intermixing lengthscale as demonstrated below.

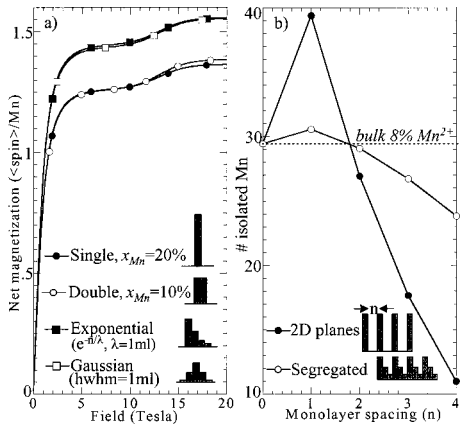

FIG. 4. (a) Calculated average magnetization (per spin) for the Mn^{2+} spin profiles shown. Despite differing intermixing profiles, the magnetization is often indistinguishable. (b) Calculated number of isolated Mn^{2+} spins (per thousand sites) assuming a 8% bulk spin distribution is redistributed as digital planes (see text). Only if planes are spaced every other monolayer is there an enhancement, although segregation greatly reduces the effect.

The model we present can also identify configurations for realizing the maximum possible magnetization per unit volume in MBE-grown structures. One motivation for growing ''digital'' alloys is to exploit the reduced clustering of 2D planes to achieve enhanced magnetizations beyond those possible with bulk, 3D distributions.[8,12] In bulk DMS, the maximum paramagnetic response is obtained with $x_{Mn} \sim 8\%$, where isolated Mn^{2+} spins comprise $\sim 2.9\%$ of all cation sites. In Fig. 4(b), we investigate whether it is then possible—*with the same total number of* Mn^{2+} *spins*—to increase the number of isolated spins by redistributing the Mn^{2+} in digital planes (solid dots). Bulk can be thought of as 2D planes of spins with $x_{Mn}^{2D}=8\%$, spaced every monolayer. Next, we consider 2D planes with twice the density ($x_{Mn}^{2D}=16\%$), spaced every other monolayer, which results in a paramagnetic enhancement of over a third, as shown. However, spacing planes with $x_{Mn}^{2D}=24\%$ every third monolayer results in *fewer* free Mn^{2+} spins per unit volume than in the case of bulk. Additional divisions continue to reduce the paramagnetic response. So, only by spacing magnetic planes every other monolayer is it possible to increase the density of free Mn^{2+} beyond 3D spin distributions. However, *any* intermixing during growth couples the 2D planes and dramatically reduces the paramagnetic enhancement, as shown by the open dots for the case of full segregation. Of course, clever schemes for control of the spin distribution *within* the 2D plane could certainly result in reduced spin clustering, such as MBE growth in the (120) direction, where neighboring cation sites in the (120) plane are *not* nearest neighbors.[12] Thusfar, however, such efforts have been hampered by the inevitable intermonolayer mixing of atoms during growth, leading to spin clusters.

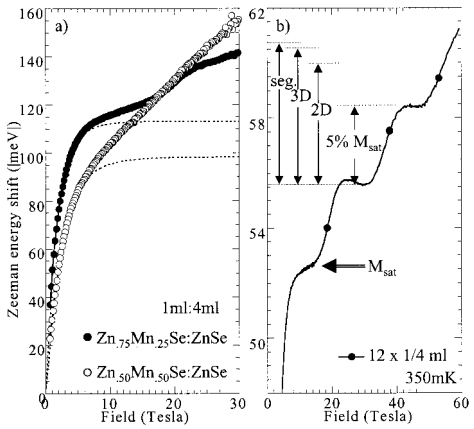

FIG. 5. (a) Measured spin splitting at 1.6 K for the two superlattices shown, from reflectivity data. Dotted lines are Brillouin function fits to the low-field data. (b) The measured magnetization steps (via PL) in the quantum well with 1/4 ml magnetic planes. The steps are smaller than any Mn^{2+} distribution would predict.

We apply the model to measurements of superlattices and quantum wells containing ''digital'' planes of DMS. Figure 5(a) shows the measured splitting between exciton spin states in two superlattices with nominally single monolayers of $Zn_{.75}Mn_{.25}Se$ and $Zn_{.50}Mn_{.50}Se$ (separated by 4 ml of ZnSe). The dotted lines are Brillouin fits to the low-field magnetization ($H<8$ T). Increased spin clustering in the $Zn_{.50}Mn_{.50}Se$ monolayers is evident in the smaller paramagnetic saturation, and more linear high-field susceptibility. With perfect 2D planes, however, it is impossible to account for the 15% larger paramagnetic saturation from the superlattice with $Zn_{.75}Mn_{.25}Se$ planes. However, assuming exponential, segregated Mn^{2+} profiles $\propto e^{-n/\lambda}$ for each of the $Zn_{1-x}Mn_xSe$ planes (reasonable for the low growth temperature of 300 C), the relative low field saturations can be reproduced with a decay length $\lambda = 1.15$ ml, implying partial segregation during growth. As a final study [Fig. 5(b)], we attempt to account for the size of the magnetization steps observed in PL from the quantum well containing twelve 1/4 ml planes of MnSe. Magnetization steps arise from the partial unlocking of antiferromagnetically bound Mn-Mn pairs, resulting in a step height proportional to the number of pairs. The observed magnetization steps are *never more than* 5% of the low-field ''saturation magnetization'' M_{sat}, a ratio that is much smaller than predicted by *any* conceivable distribution profile of the Mn^{2+} within the quantum well. The expected step height for 3D, 2D, and segregated 2D spin distributions are shown for comparison. This puzzling anomaly is seen in all ''digital'' samples, and even quantum wells containing bulk ($x_{\mathrm{Mn}}^{\mathrm{3D}}=8\%$) DMS show a similar deficit. We postulate this effect is due to the nature of the PL measurement itself, which is not a direct measure of magnetization, but is rather only proportional to the magnetization through the $J_{sp\text{-}d}$ exchange interaction and the Mn^{2+}-exciton wavefunction overlap. It is anticipated that true magnetization studies will reveal the correct magnitude of the magnetization step.

In summary, we have presented a method for calculating the exact number of spin singles, pairs, triples, and higher-order clusters for an arbitrary magnetic concentration profile in the (100) growth direction, to model the magnetic properties of real, quasi-2D spin distributions in DMS heterostructures. Calculation of the magnetization for diffusion and segregation profiles reveals nearly identical values, so that fitting an intermixing length is likely possible only when the form (exponential, gaussian, etc) of the quasi-2D profile is assumed *a priori*, as was demonstrated for the case of $Zn_{1-x}Mn_xSe$:ZnSe superlattices. The model also predicts a larger paramagnetism compared with bulk spin distributions *only* if digital planes are spaced every other monolayer, although the effects of intermixing will greatly reduce any enhancement. Lastly, the discrepancy between the magnitude of observed and predicted magnetization steps remains outstanding. The methods outlined in this paper will be of use in modeling future epitaxially grown DMS heterostructures, where spin distributions can be engineered with nearly monolayer precision.

The authors gratefully acknowledge the assistance of J. Schillig and M. Gordon during operation of the 60T Long-Pulse magnet. Work supported by Grants Nos. NSF DMR 97-01072 and 9701484.

[1] Y. Shapira, J. Appl. Phys. **67**, 5090 (1990); Y. Shapira *et al.*, Phys. Rev. B **33**, 356 (1986); **30**, 4021 (1984).
[2] W. Grieshaber *et al.*, Phys. Rev. B **53**, 4891 (1996); **50**, 2011 (1994).
[3] J. A. Gaj *et al.*, Phys. Rev. B **50**, 5512 (1994).
[4] W. Ossau, B. Kuhn-Heinrich, A. Waag, and G. Landwehr, J. Cryst. Growth **159**, 1046 (1996).
[5] A. Lemaitre *et al.*, Phys. Rev. B **57**, 4708 (1998).
[6] X. Wang, D. Heiman, S. Foner, and P. Becla, Phys. Rev. B **41**, 1135 (1990).
[7] S. A. Crooker *et al.*, Phys. Rev. B **60**, R2173 (1999); Phys. Rev. Lett. **75**, 505 (1995).
[8] J. K. Furdyna, J. Appl. Phys. **64**, R29 (1988).
[9] P. Harrison, J. M. Fatah, T. Stirner, and W. E. Hagston, J. Appl. Phys. **79**, 1684 (1996).
[10] M. T. Liu *et al.*, Phys. Rev. B **54**, 6457 (1996).
[11] V. Bindilatti *et al.*, J. Appl. Phys. **85**, 5950 (1999).
[12] R. Fiederling *et al.*, Phys. Rev. B **58**, 4785 (1998); M. Kutrowski *et al.*, Thin Solid Films **306**, 283 (1997).